Electronic structure of perovskite-type compounds

Michihide Kitamura and Shinji Muramatsu
Department of Electrical and Electronic Engineering, Faculty of Engineering, Utsunomiya University, 2753 Ishii-machi, Utsunomiya, Tochigi 321, Japan
(Received 20 July 1989)

Band structures are calculated for perovskite-type compounds KMF_3 (with M = Mn, Fe, Co, Ni, Cu, and Zn) on the basis of the extended Hückel tight-binding method and a partial density of states as well as a total density of states is presented for comparison with available experimental data. Our calculations, which are entirely based on first principles in the sense that empirical atomic data are not used, explain fairly well experiments obtained from ultraviolet photoelectron and x-ray spectroscopies. The important role of potassium ions in conduction bands is pointed out and discussed in connection with a multiple-scattering approach to x-ray-absorption processes reported previously.

I. INTRODUCTION

Perovskite fluorides with a transition-metal ion have been extensively studied both experimentally and theoretically.[1-7] Our intention in this paper is to obtain a further understanding of the electronic band structures for these materials through a comparative study of theoretical calculations of the band structures and experimental data obtained from ultraviolet photoelectron spectroscopy (UPS) and x-ray spectroscopy. Onuki *et al.* measured UPS spectra of perovskite fluorides KMF_3 (with M=Mn, Fe, Co, Ni, Cu, and Zn) in the valence-band region,[7] and analyzed them in terms of the calculation of M $3d^{n-1}$ multiplets including the ligand field. For x-ray data, Shulman *et al.* obtained metal K x-ray-absorption spectra from KMF_3 (with M=Mn, Fe, Co, Ni, and Zn);[6] and Kawada measured F $K\alpha$ emission spectra for $KNiF_3$ and $KCuF_3$.[8] We will use these experimental data as a test of the band-structure calculations presented in this work.

We have so far studied the x-ray-absorption near-edge structure (XANES), which provides information on conduction bands, on the basis of a multiple-scattering (MS) theory within a muffin-tin approximation.[9-14] On the other hand, in order to mainly obtain information on valence bands, very recently, we have carried out molecular-orbital (MO) calculations for a $(PdCl_6)^{2-}$ cluster in a K_2PdCl_6 crystal, using a self-consistent-charge extended Hückel method.[15] The present work is an extension of this MO calculation. We calculate the electronic band structures for KMF_3 (with M=Mn, Fe, Co, Ni, Cu, and Zn) using the extended Hückel tight-binding (XHTB) method,[16] and obtain the partial density of states as well as the total density of states. The latter is compared with the UPS spectra, while the former with the x-ray spectra. We also present x-ray spectra obtained from MO calculations and discuss how different features appear between spectra obtained from the band-structure and MO calculations. The point to be noted on our calculations is that empirical atomic data are not used. In such a sense our calculations are entirely based on first principles. The comparison between different experiments (UPS and x-ray spectroscopy) and the calculation will provide the stringent test of our theoretical approach based on the XHTB method, which is expected to work well in ionic crystals such as KMF_3.

In Sec. II we briefly describe our calculational method. In Sec. III A the result for $KNiF_3$ is presented and discussed in connection with UPS and x-ray spectra, and compared with theoretical calculations by Mattheiss.[5] The results for other materials are shown in Sec. III B and discussion is concentrated on the difference among the band structures of different materials.

II. THEORY

In this section we briefly sketch the extended Hückel tight-binding method and describe a practical procedure. We solve the following Schrödinger equation:

$$H\Psi_{\mathbf{k}}(\mathbf{r})=E_{\mathbf{k}}\Psi_{\mathbf{k}}(\mathbf{r}) , \tag{1}$$

where H is a one-electron Hamiltonian consisting of a kinetic-energy term and the crystal potential, which is periodic with the periodicity of the lattice. The one-electron wave function $\Psi_{\mathbf{k}}(\mathbf{r})$ is specified by a wave vector $\mathbf{k}$ within the first Brillouin zone (BZ). According to the Bloch theorem in the tight-binding scheme it is written as

$$\Psi_{\mathbf{k}}(\mathbf{r})=\sum_{\mu}\sum_{L} u_L^{(\mu)}(\mathbf{k})\chi_L^{(\mu)}(\mathbf{k},\mathbf{r}) , \tag{2a}$$

$$\chi_L^{(\mu)}(\mathbf{k},\mathbf{r})=\sum_{\mathbf{r}_\mu} e^{i\mathbf{k}\cdot\mathbf{r}_\mu}\phi_L^{(\mu)}(\mathbf{r}-\mathbf{r}_\mu)/\sqrt{N_\mu} , \tag{2b}$$

where summation over μ is taken for five independent K, M, F(1), F(2), and F(3) ions [see Fig. 1 for F(1), F(2), and F(3)]; $\mathbf{r}_\mu$ denotes their positions throughout the crystal. Here, $\phi_L^{(\mu)}(\mathbf{r}-\mathbf{r}_\mu)$ is the atomic orbital with a quantum state denoted by the collective index $L=(l,m)$ for the μ ion located at $\mathbf{r}_\mu$. The quantum number l contains a principal quantum number in addition to usual orbital-angular-momentum quantum number l, and m denotes its

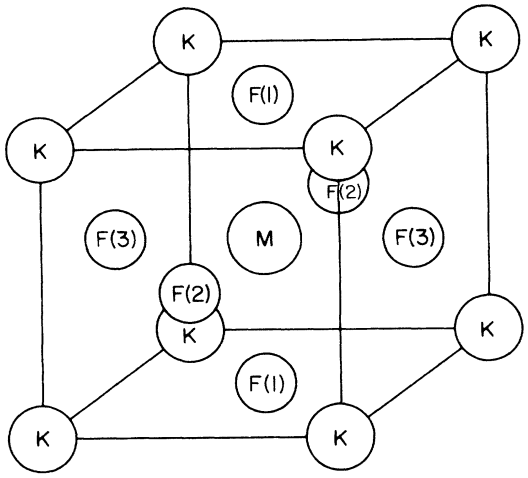

FIG. 1. Unit cell for perovskite-type compound KMF_3. Three different types of fluorine ions are indicated by F(1), F(2), and F(3).

degenerate components for a real base. For example, $L=(2p,x)$, $(3d, x^2-y^2)$, etc. N_μ is the number of the μ ion, being equal to $N/5$, where N is the total number of the ions constituting the compound KMF_3. The coefficient $u_L^{(\mu)}(\mathbf{k})$ and energy $E_\mathbf{k}$ are obtained as a function of the wave vector $\mathbf{k}$ by solving the following secular equation:

$$\mathbf{H}(\mathbf{k})\mathbf{u}(\mathbf{k})=E_\mathbf{k}\mathbf{S}(\mathbf{k})\mathbf{u}(\mathbf{k}) , \tag{3a}$$

where $\mathbf{u}(\mathbf{k})=(\ldots,u_L^{(\mu)},\ldots,u_{L'}^{(\nu)},\ldots)^\tau$, and $\mathbf{H}(\mathbf{k})$ and $\mathbf{S}(\mathbf{k})$ are matrices whose elements are given as follows:

$$H_{L,L'}^{(\mu),(\nu)}(\mathbf{k})=\langle\chi_L^{(\mu)}(\mathbf{k},\mathbf{r})|\mathbf{H}|\chi_{L'}^{(\nu)}(\mathbf{k},\mathbf{r})\rangle = \sum_{\mathbf{r}_\nu} e^{i\mathbf{k}\cdot\mathbf{r}_\nu}\langle\phi_L^{(\mu)}(\mathbf{r})|\mathbf{H}|\phi_{L'}^{(\nu)}(\mathbf{r}-\mathbf{r}_\nu)\rangle , \tag{3b}$$

$$S_{L,L'}^{(\mu),(\nu)}(\mathbf{k})=\langle\chi_L^{(\mu)}(\mathbf{k},\mathbf{r})|\chi_{L'}^{(\nu)}(\mathbf{k},\mathbf{r})\rangle = \sum_{\mathbf{r}_\nu} e^{i\mathbf{k}\cdot\mathbf{r}_\nu}\langle\phi_L^{(\mu)}(\mathbf{r})|\phi_{L'}^{(\nu)}(\mathbf{r}-\mathbf{r}_\nu)\rangle . \tag{3c}$$

In the evaluation for the matrix elements of H given by Eq. (3b), we use the Wolfsberg-Helmholtz approximation,[17]

$$\langle\phi_L^{(\mu)}(\mathbf{r})|\mathbf{H}|\phi_{L'}^{(\nu)}(\mathbf{r}-\mathbf{r}_\nu)\rangle =(G/2)(\varepsilon_L^{(\mu)}+\varepsilon_{L'}^{(\nu)})\langle\phi_L^{(\mu)}(\mathbf{r})|\phi_{L'}^{(\nu)}(\mathbf{r}-\mathbf{r}_\nu)\rangle , \tag{4}$$

where G is an adjustable parameter and $\varepsilon_L^{(\mu)}$ is the Madelung corrected atomic energy for the L state of the μ ion. We calculated the Madelung correction with Evjen's method.[18] The overlap integral

$$\langle\phi_L^{(\mu)}(\mathbf{r})|\phi_{L'}^{(\nu)}(\mathbf{r}-\mathbf{r}_\nu)\rangle\equiv\Delta_{L,L'}^{\mu,\nu}(\mathbf{r}_\nu)$$

can be transformed into basic overlap integrals $[\Delta_{sp\sigma}^{\mu,\nu}(r_\nu),\Delta_{pp\sigma}^{\mu,\nu}(r_\nu),\Delta_{pp\pi}^{\mu,\nu}(r_\nu),\ldots]$ by use of direction cosine (α,β,γ) of $\mathbf{r}_\nu$, as shown in the table of Slater and Koster.[19] For example, $\Delta_{p_x,d_{xy}}^{\mu,\nu}(\mathbf{r}_\nu)$ is expanded as $\sqrt{3}\alpha^2\beta\Delta_{pd\sigma}^{\mu,\nu}(r_\nu)+\beta(1-2\alpha^2)\Delta_{pd\pi}^{\mu,\nu}(r_\nu)$. Here, $\Delta_{pd\sigma}^{\mu,\nu}(r_\nu)$ and $\Delta_{pd\pi}^{\mu,\nu}(r_\nu)$ denote, respectively, the overlap integrals for σ and π states between the p orbital of the μ ion located on (0,0,0) and the d orbital of the ν ion located on $(0,0,r_\nu)$. We numerically calculated these integrals by use of elliptic coordinates.[20]

The main objective of this paper is to calculate both the total and partial densities of states, in order to make a comparison with UPS and x-ray data. The total density of states $D(E)$ (TDOS) is defined as the number of allowed levels per unit volume per unit energy range,

$$D(E)=2\sum_{\mathbf{k}}^{\Omega}\delta(E-E_\mathbf{k}) , \quad =2\sum_{\mathbf{k}}^{\Omega/48} g(\mathbf{k})\delta(E-E_\mathbf{k}) . \tag{5a}$$

Similarly, the partial density of states $P_l^{(\mu)}(E)$ (PDOS) for the l state of the μ ion is defined as follows:

$$P_l^{(\mu)}(E)=2\sum_{\mathbf{k}}^{\Omega/48} g(\mathbf{k})\sum_m |u_L^{(\mu)}(\mathbf{k})|^2\delta(E-E_\mathbf{k}) . \tag{5b}$$

Here, $g(\mathbf{k})$ denotes the number of the so-called "star of $\mathbf{k}$," and $\Omega/48$ is the volume surrounded by symmetry points Γ, X, M, and R in the first BZ with the volume of Ω and defined by $0\le k_z\le k_y\le k_x\le 1$ in units of π/a_0. The $g(\mathbf{k})$ which is necessary to practical computations is listed in Table I. We note that the PDOS in (5b) is proportional to the x-ray absorption or emission spectrum. For instance, the $P_{4p}^{(M)}$ is proportional to the metal K x-ray-absorption spectrum with which we are concerned in the present paper. Following a widely used procedure, we represent the density of states in terms of histograms $D(E_i)$ and $P_l^{(\mu)}(E_i)$, where the subscript i in E_i means a discrete energy variable instead of the continuous energy variable E. The histogram is related to $D(E)$ or $P_l^{(\mu)}(E)$ by the following equations:

$$D(E_i)\Delta E=\int_{E_i-\Delta E/2}^{E_i+\Delta E/2} D(E')dE' , \tag{6a}$$

and

$$P_l^{(\mu)}(E_i)\Delta E=\int_{E_i-\Delta E/2}^{E_i+\Delta E/2} P_l^{(\mu)}(E')dE' , \tag{6b}$$

TABLE I. The number $g(\mathbf{k})$ of $\mathbf{k}$ vectors in the stars for the wave number $\mathbf{k}$ defined within the volume surrounded by symmetry points Γ, X, M, and R shown in Fig. 2. Π_{XMR} is a triangle made from three points X, M, and R.

$\mathbf{k}$	Γ	X	M	R	Δ	Z	Σ	T	Λ	S	Π_{XMR}	otherwise
$g(\mathbf{k})$	1	3	3	1	6	12	12	6	8	12	24	48

where ΔE is the width of the histograms and it is chosen to be 0.5 eV throughout this paper.

Theoretical details for MO calculations have been described in our previous paper.[15] Here, we will not repeat them, but mention a different point from the previous treatment. In the present MO calculations we fixed the charges of K, M, and F ions as $+1$, $+2$, and -1, respectively, without taking into account a charge transfer. Our calculation corresponds to a cluster of $(MF_6)^{4-}$.

Next, let us proceed to practical details. Input data for calculations are Herman-Skillman's atomic data,[21] lattice constants, and the value of the adjustable parameter G. Starting from a self-consistent-field (SCF) calculation[10–15,20] based on the prescription of Herman and Skillman with the use of Schwarz's exchange-correlation parameters[22] for atoms, we have obtained atomic orbitals which are used to carry out the band-structure and MO calculations. These are $3p$ and $4s$ orbitals for $K^+(1s^2 2s^2 2p^6 3s^2 3p^6 4s^0)$; $3d$, $4s$, and $4p$ ones for $M^{2+}(1s^2 2s^2 2p^6 3s^2 3p^6 3d^n 4s^0 4p^0)$; and $2s$ and $2p$ ones for $F^-(1s^2 2s^2 2p^6)$. Here, the number n of electrons on the $3d$ orbital is 5, 6, 7, 8, 9, and 10 for M=Mn, Fe, Co, Ni, Cu, and Zn, respectively.

The unit cell of perovskite-type compounds KMF_3 contains an M ion at the body center, F ions at each of the face center, and K ions at the corners of a simple cubic unit cell, as shown in Fig. 1. The primitive lattice vectors t_1, t_2, and t_3 for this structure are $(a_0,0,0)$, $(0,a_0,0)$, and $(0,0,a_0)$, respectively, where a_0 is a lattice constant. For fluorine ions, there are three types of independent sites, which are denoted by F(1), F(2), and F(3) in Fig. 1. The reciprocal lattice vectors $\mathbf{k}_1$, $\mathbf{k}_2$, and $\mathbf{k}_3$ are given as (1,0,0), (0,1,0), and (0,0,1) in units of $2\pi/a_0$. The first BZ is shown in Fig. 2, where symmetry points $\Gamma(0,0,0)$, $X(1,0,0)$, $M(1,1,0)$, and $R(1,1,1)$ are also indicated in units of π/a_0 along with symmetry axes $\Delta(x,0,0)$, $Z(1,x,0)$, $\Sigma(x,x,0)$, $T(1,1,x)$, $\Lambda(x,x,x)$, and $S(1,x,x)$, x being in the range $0<x<1$.

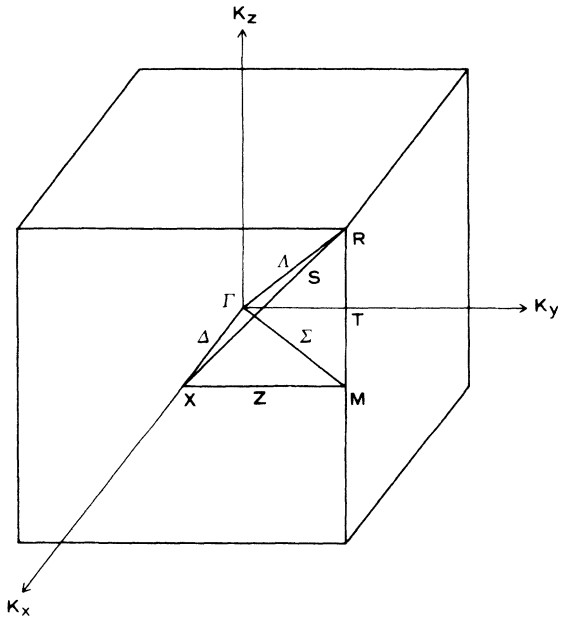

FIG. 2. Brillouin zone for a simple cubic Bravais lattice.

The matrix element for $\mathbf{H}$ given by Eq. (4) contains the atomic energy $\varepsilon_L^{(\mu)}$ corrected by the Madelung energy which is expressed as $(2/a_0)\sigma_\mu$ ($\mu=K^+$, M^{2+}, and F^-) in atomic units. The values of σ_μ for the perovskite-type compound KMF_3 are 2.695, 6.194, and -3.233 for $\mu=K^+$, M^{2+}, and F^-, respectively; and the values of the lattice constant a_0 are 4.190, 4.122, 4.069, 4.012, and 4.055 Å for M=Mn, Fe, Co, Ni, and Zn, respectively.[23] The crystal structure of $KCuF_3$ is tetragonal, being different from that of the others and has a_0 of 4.140 Å and c_0 of 3.926 Å.[23] For simplicity, we regard its crystal structure as a cubic one having a_0 of 4.0 Å which nearly equals the average of real values of a_0 and c_0.

Finally we mention the adjustable parameter G appearing in the matrix elements. For the energy band of $KNiF_3$ and MO of $(NiF_6)^{4-}$, we checked two types of G: $G=1.75$ (Ref. 24) and $G=2-|\Delta|$ (Ref. 25), which were used in our previous work.[15] These results almost did not depend on the values of G, as in our previous work. Nevertheless, the value of $G=1.75$ gave a better result of $10Dq$ for the MO calculation than $G=2-|\Delta|$. We decided to use $G=1.75$ throughout this paper.

III. RESULTS AND DISCUSSION

Before presenting the results of band-structure calculations, we would like to make a comment on the basic overlap integrals ($\Delta_{ss\sigma}^{\mu,\nu}$, $\Delta_{sp\sigma}^{\mu,\nu}$, ...). The matrix elements of $\mathbf{H}$ and $\mathbf{S}$ contain these overlap integrals depending on the distance between ions on which atomic orbitals are located. In order to obtain the accurate values of these matrix elements, it is necessary to carry out the summation over $\mathbf{r}_\nu$ [see Eqs. (3b) and (3c)] up to a sufficiently large distance until the absolute values of the basic overlap integrals become negligibly small ($<10^{-6}$). In order to show how they decay as a function of the distance between ions we list the absolute values of the basic overlap integrals for $KNiF_3$ in Appendix A, where shell structures and Madelung corrections for the perovskite-type compounds are also tabulated. For example, the fifth column in Table III gives the value of $|\Delta_{sp\sigma}^{N_i,\nu}|$ for ν=K, Ni, or F. The value between Ni and F ions changes as 2.848×10^{-1}, 2.839×10^{-2}, 2.176×10^{-3}, 1.277×10^{-4}, and 3.187×10^{-6}, respectively, in going to the first, fourth, sixth, ninth, and eleventh shells of F ions surrounding the Ni ion located at the center. In practical calculations of the matrix elements of $\mathbf{H}$ and $\mathbf{S}$, we included all the overlap integrals between the ions distant from each other up to $3a_0$, which yielded a sufficient accuracy.

A. $KNiF_3$

In this section we discuss the results for $KNiF_3$ in detail, because for this compound experimental data are most readily available and a band-structure calculation has been reported. MO calculations for the $(NiF_6)^{4-}$ cluster are compared with a hypothetical band-structure calculation, in which the contribution of potassium ions is neglected intentionally with no change of others such

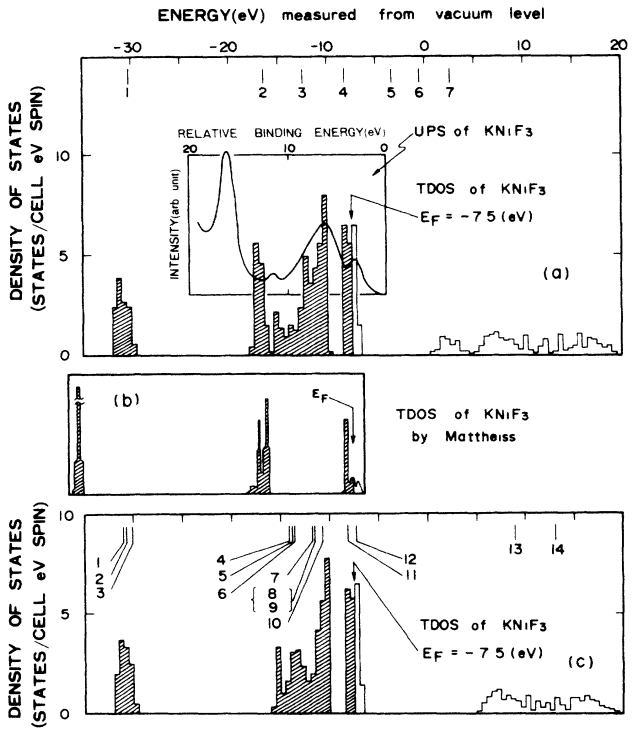

FIG. 3. Total density of states (TDOS) for $KNiF_3$. (a) The TDOS calculated by taking into account $3p$ and $4s$ orbitals of K^+, $3d$, $4s$, and $4p$ ones of Ni^{2+} and $2s$ and $2p$ ones of F^- ions, on the basis of the extended Hückel tight-binding (XHTB) method. This figure includes an ultraviolet photoelectron spectroscopy (UPS) spectrum observed by Onuki *et al.* in the valence band region, and Madelung corrected atomic energies $\varepsilon_L^{(\mu)}$ for atomic orbitals used in the calculation. The $\varepsilon_L^{(\mu)}$ levels are indicated by the numbers from 1 to 7, which correspond to $F^-(2s)$, $K^+(3p)$, $F^-(2p)$, $Ni^{2+}(3d)$, $Ni^{2+}(4s)$, $K^+(4s)$, and $Ni^{2+}(4p)$, respectively. (b) The TDOS calculated by Mattheiss by the APW method. (c) The TDOS calculated by the XHTB method for a hypothetical crystal, in which K^+ ions are neglected. Molecular-orbital (MO) levels obtained from the MO calculation based on the extended Hückel method are also indicated. The MO levels are denoted by the numbers from 1 to 14, which correspond to $1a_{1g}$, $1t_{1u}$, $1e_g$, $2a_{1g}$, $2t_{1u}$, $1t_{2g}$, $1t_{2u}$, $2e_g$, $3t_{1u}$, $1t_{1g}$, $2t_{2g}$, $3e_g$, $3a_{1g}$, and $4t_{1u}$, respectively.

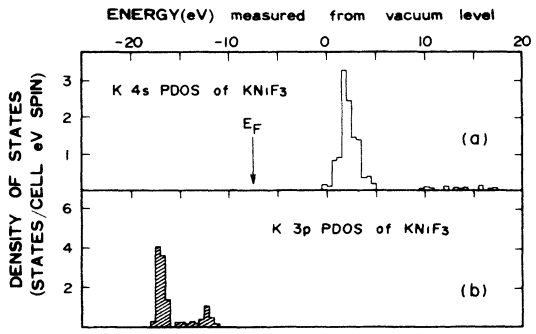

FIG. 4. Partial density of states (PDOS) for (a) $4s$ orbital and (b) $3p$ orbital of K^+ ion in $KNiF_3$.

as a crystal structure. The calculated results of TDOS for $KNiF_3$ are shown in Figs. 3(a) and 3(c), and the experimental UPS spectrum is compared with the TDOS in Fig. 3(a). For comparison, the result based on the augmented-plane-wave (APW) method by Mattheiss[5] is also displayed in Fig. 3(b). The TDOS in Fig. 3(c) is the result obtained by neglecting the K^+ ions. Madelung corrected atomic energy $\varepsilon_L^{(\mu)}$ and the energy level of the MO are also indicated in Figs. 3(a) and 3(c), respectively. The result of PDOS, $P_l^{(\mu)}(E_i)$, is shown in Fig. 4 for ($\mu = K^+$; $l = 4s$ and $3p$), in Fig. 5 for ($\mu = Ni^{2+}$; $l = 4s$, $4p$, and $3d$), and in Fig. 6 for ($\mu = F^-$, $l = 2s$ and $2p$). The experimental Ni K x-ray absorption[6] and F $K\alpha$ emission spectra[8] are drawn in Figs. 5 and 6, respectively. The PDOS's in Figs. 5(d), 5(e), and 5(f) and Figs. 6(c) and 6(d) are the results for hypothetical calculations.

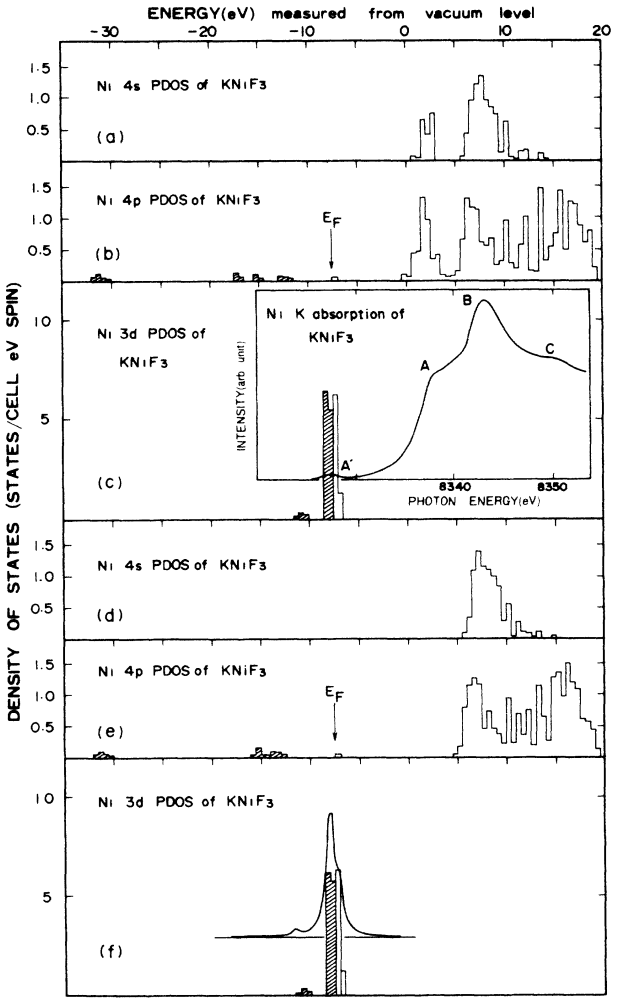

FIG. 5. Partial density of states (PDOS) for $4s$, $4p$, and $3d$ orbitals of Ni^{2+} ion in $KNiF_3$. (a) and (d) stand for the PDOS of the $4s$ orbital, (b) and (e) for that of the $4p$ one, and (c) and (f) for that of the $3d$ one. (d), (e), and (f) are the results calculated by neglecting the K^+ ions. Ni K x-ray-absorption spectrum observed by Shulman *et al.*, which is to be compared with the Ni $4p$ PDOS of $KNiF_3$ in (b), is drawn in (c). Ni $L\alpha$ emission spectra calculated by use of the results of the MO is also illustrated in (f).

First let us discuss the valence band, which consists of three parts, lower, middle, and upper bands, as seen from Fig. 3(a). The partial density of states $P_{2s}^{(F)}$ in Fig. 6(a) indicates that the lower band mainly comes from the F $2s$ state. The upper band is made up of Ni $3d$ states, as seen from $P_{3d}^{(Ni)}$ in Fig. 5(c). We will call the former and latter bands fluorine $2s$ and metal $3d$ bands, respectively. The TDOS for the middle band is composed of two peaks. The lower peak mainly consists of $P_{3p}^{(K)}$ [Fig. 4(b)] and $P_{2p}^{(F)}$ [Fig. 6(b)]. However, considering the fact that the contribution of the F $2p$ state to the TDOS [Fig. 3(a)] around -17 eV is induced by K ions as seen from comparison of Figs. 6(b) and 6(d), we can regard the lower-energy part of the middle band as K $3p$ band. The remainder of the middle band is mainly built up from F $2p$ states as seen from Fig. 6(b), so we call it a F $2p$ band. Mattheiss's valence band shown in Fig. 3(b) also consists

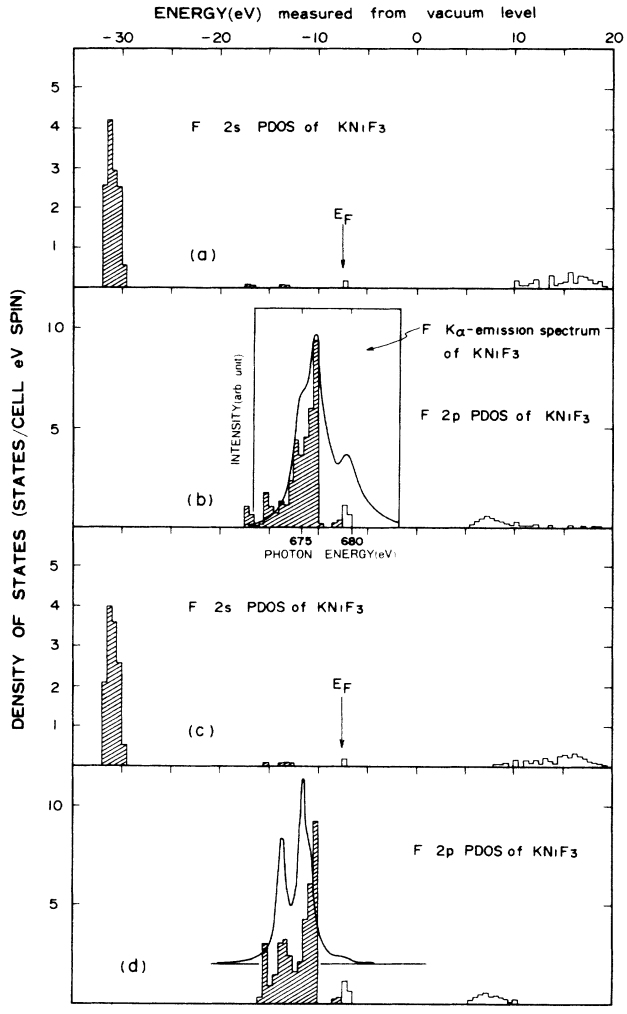

FIG. 6. Partial density of states (PDOS) for $2s$ and $2p$ orbitals of F^- ion in $KNiF_3$. (a) and (c) show the PDOS for the $2s$ orbital and (b) and (d) that for the $2p$ one. (c) and (d) are the PDOS calculated by neglecting the K^+ ions. F $K\alpha$ emission spectrum measured by Kawada and that calculated from the MO are displayed in (b) and (d), respectively, for comparison.

of three bands, but his band corresponding to our middle band is very narrow as compared to ours. However, its profile is quite similar to that of ours. The UPS spectrum measured by Onuki *et al.* is compared with our TDOS in Fig. 3(a). They have ascribed the peak at about 16 eV and the band around 6 eV, in the energy scale of relative binding energy (RBE), to the K $3p$ level and the F $2p$ valence band, respectively. These interpretations are consistent with our results of calculations. The correspondence between experiment and calculation is nice, except for a shift of the peak at about 16 eV in RBE. This shift is common to all the compounds, as shown below. In Fig. 6(b) the PDOS for F $2p$ states is compared with the observed F $K\alpha$ emission spectrum. This comparison indicates that the calculation fairly well reproduces the experimental result. However, agreement for the high-energy peak is rather poor. This may be an indication of a many-body effect near the Fermi level.

Next we discuss the result of MO calculations in connection with the hypothetical band structure. The MO energy levels for a $(NiF_6)^{4-}$ cluster are shown in Fig. 3(c). These energy positions fairly well correspond to broadened bands for the hypothetical band-structure calculation. It is instructive to point out that the Fermi level (E_F^m) deduced from MO calculation is nearly equal to that from the band structure (E_F^b), that is, $E_F^m = -7.22$ eV and $E_F^b = -7.5$ eV for $KNiF_3$. For comparison we describe here these values for the other compounds: $E_F^m = -4.88$ eV, $E_F^b = -5.0$ eV for $KMnF_3$; $E_F^m = -5.92$ eV, $E_F^b = -5.5$ eV for $KFeF_3$; $E_F^m = -6.28$ eV, $E_F^b = -6.5$ eV for $KCoF_3$; $E_F^m = -8.20$ eV, $E_F^b = -8.0$ eV for $KCuF_3$; and $E_F^m = -9.67$ eV, $E_F^b = -8.5$ eV for $KZnF_3$ (see Appendix B for details of the results of MO calculations). In order to compare the MO calculation with the x-ray experiment and the PDOS of the hypothetical band-structure calculation, we have calculated F $K\alpha$ and Ni $L\alpha$ emission spectra using the MO results under an assumption of the Lorentzian broadening with the width of 1.0 eV. They are shown in Figs. 6(d) and 5(f). The F $K\alpha$ emission spectrum [solid curve in Fig. 6(d)] obtained from the MO calculation provides a qualitative explanation of the experiment [solid curve in Fig. 6(b)]. From these observations, electronic properties originating from only transition-metal and fluorine ions may be qualitatively understood from a picture of MO for a $(MF_6)^{4-}$ cluster. However, we will demonstrate in the next paragraph that potassium ions make an indirect but important contribution to the electronic properties associated with the transition-metal or fluorine ions in the conduction band region.

Finally, let us now proceed to discuss the conduction band, which is calculated in the energy range of about 20 eV. Roughly speaking, it is divided into three parts, lower, middle, and upper ones. From PDOS for each atom we see that the lower band is mainly made up of K $4s$, Ni $4s$, and Ni $4p$ states, the middle one of Ni $4s$ and $4p$ and F $2p$ states, and the upper one of Ni $4p$ and F $2s$ states. We notice that the whole of the lower band is missing in the hypothetical band structure [Fig. 3(c)]. This implies that potassium ions play an important role in the formation of the lower band, which is composed of

K 4*s*, Ni 4*s*, and Ni 4*p* states. The PDOS of K 4*s* [Fig. 4(a)] shows that the contribution of the K 4*s* state to the lower band is dominant, and from Figs. 5(a), 5(b), 5(d), and 5(e) it is found that the K 4*s* state induces admixtures of Ni 4*s* and 4*p* states into itself. Here, we compare the Ni K x-ray-absorption spectrum observed by Shulman *et al.* [which is drawn in the inset in Fig. 5(c)] with our calculated result for the PDOS of Ni 4*p* shown in Fig. 5(b). In the energy region within about 20 eV, this x-ray spectrum has a small peak *A'* and the main peak *B* accompanied with a structure *A* at the low-energy side and with a structure *C* at the high-energy side. The calculated PDOS of Ni 4*p* [Fig. 5(b)] fairly well reproduces such experimental features including a small peak *A'*. The features *A*, *B*, and *C* correspond, respectively, to the lower, middle, and upper bands, which all contain the Ni 4*p* states. A small peak *A'* is caused by the mixing of the Ni *p* states into the 3*d* bands. This will be mentioned again in the discussion of the result for $KZnF_3$. We should like to emphasize that the structure *A* is induced by the K 4*s* state. The nature of the structure *A* has been already shown to have an *s* character in our previous work,[12] where the metal K x-ray-absorption spectra for KMF_3 (M=Mn, Fe, Co, Ni, and Zn) have been calculated in the energy region within about 60 eV of the absorption threshold by using the MS approach. Therefore we can state that the calculation without the contribution of K atoms does not give a complete explanation of the experiment on the metal K x-ray absorption. Our recent calculation based on the MS theory for a single cluster of Co^{3+} complex compounds confirms this statement.[14] A structure observed experimentally at the low-energy side of the main peak for the Co K x-ray absorption is missing in our spectrum calculated for a single cluster, for example, $[Co(NH_3)_6]^{3+}$. We showed that the structure appearing at the low-energy side of the main peak is connected with the scattering effect from atoms outside a single cluster, doing the MS calculation in which the atoms

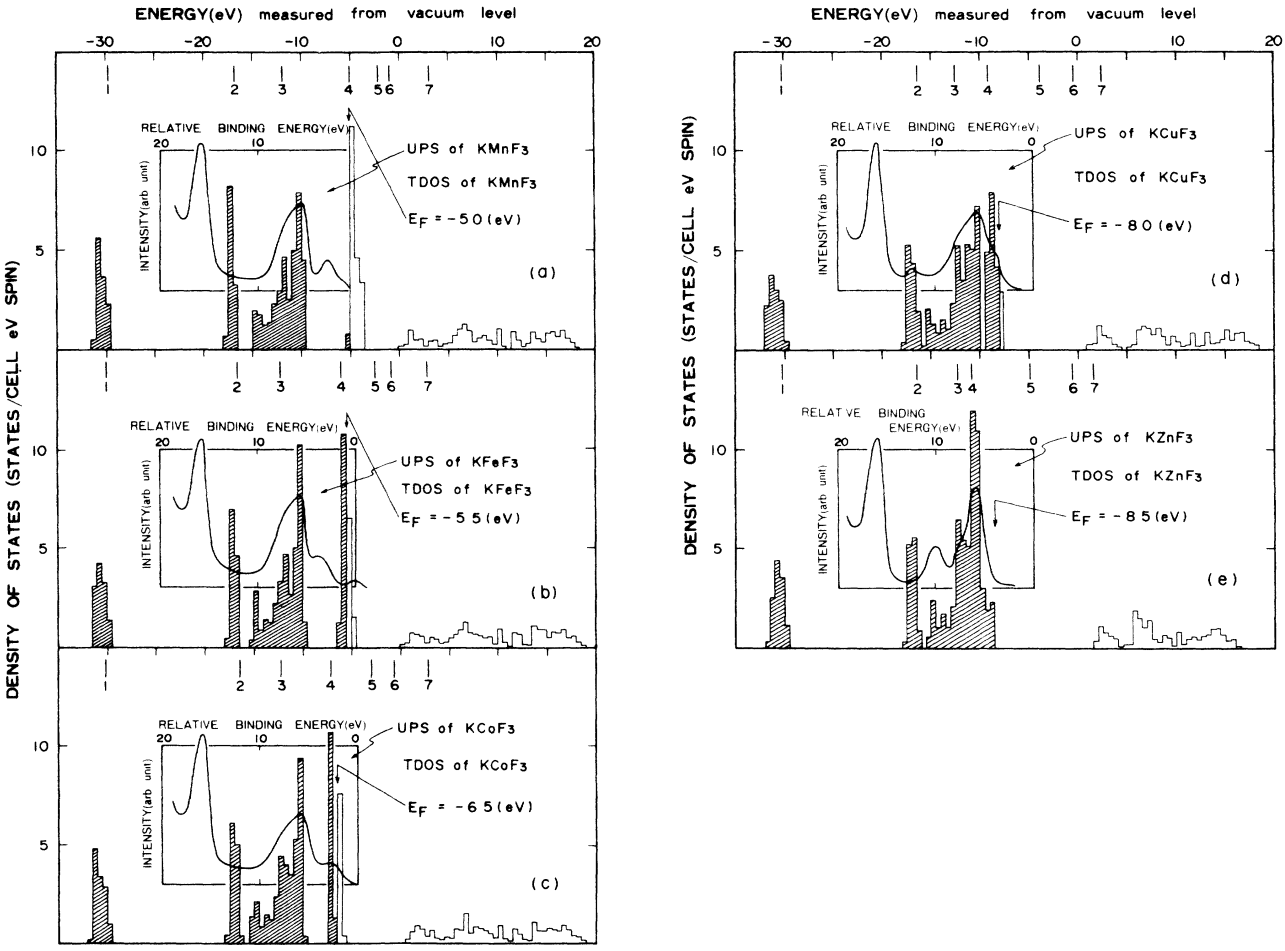

FIG. 7. Total density of states (TDOS) for (a) $KMnF_3$, (b) $KFeF_3$, (c) $KCoF_3$, (d) $KCuF_3$, and (e) $KZnF_3$. For comparison, the Madelung corrected atomic energies $\varepsilon_L^{(\mu)}$ for the used orbitals are indicated, and the UPS spectra observed by Onuki *et al.* are also drawn. In (a)–(e) the $\varepsilon_L^{(\mu)}$ levels are indicated by the numbers from 1 to 7, which correspond to (a) $F^-(2s)$, $K^+(3p)$, $F^-(2p)$, $Mn^{2+}(3d)$, $Mn^{2+}(4s)$, $K^+(4s)$, and $Mn^{2+}(4p)$; (b) $F^-(2s)$, $K^+(3p)$, $F^-(2p)$, $Fe^{2+}(3d)$, $Fe^{2+}(4s)$, $K^+(4s)$, and $Fe^{2+}(4p)$; (c) $F^-(2s)$, $K^+(3p)$, $F^-(2p)$, $Co^{2+}(3d)$, $Co^{2+}(4s)$, $K^+(4s)$, and $Co^{2+}(4p)$; (d) $F^-(2s)$, $K^+(3p)$, $F^-(2p)$, $Cu^{2+}(3d)$, $Cu^{2+}(4s)$, $K^+(4s)$, and $Cu^{2+}(4p)$; and (e) $F^-(2s)$, $K^+(3p)$, $F^-(2p)$, $Zn^{2+}(3d)$, $Zn^{2+}(4s)$, $K^+(4s)$, and $Zn^{2+}(4p)$.

outside a cluster are taken into account. Since in $KNiF_3$ under consideration the atoms outside a $(NiF_6)^{4-}$ cluster are just potassium ions, they are closely related to the structure A appearing at the low-energy side of the main peak B. It is interesting that two different approaches of the MS and band theories lead us to the same conclusion about the important role of next-nearest neighbors of the atom under excitations.

B. KMF_3 (M=Mn, Fe, Co, Cu, and Zn)

In this section we discuss the results for the other compounds KMF_3 (M=Mn, Fe, Co, Cu, and Zn), presenting the calculated TDOS and PDOS along with available experimental data. The results for the MO are given in Appendix B. The calculated TDOS are shown together with the observed UPS data in Fig. 7, where the Madelung corrected atomic energies $\varepsilon_L^{(\mu)}$ are also shown. Figures 7(a)–7(e) correspond to M=Mn, Fe, Co, Cu, and Zn, respectively. The comparisons between the TDOS and UPS data indicate that the experimental peak at about 16 eV in RBE systematically shifts to a large binding energy side from the present predicted peak position. If we accept this discrepancy for the peak energy of about 3 eV, our calculated TDOS's generally predict the UPS spectra. We are interested in investigating to what extent one-electron band theory can reproduce the UPS spectra whose explanation would require the ligand-field theory of d-electron multiplets. The fine structures observed around the d band seem to require a treatment based on such a ligand-field theory. However, we should point out that our calculations well predict the following experimentally observed characteristic features: (1) in $KCuF_3$ and $KZnF_3$ no resolved peak is observed at the low binding energy side of the peak at about 6 eV in RBE, while in the other compounds peaks are clearly resolved around it; and (2) in $KNiF_3$, $KCuF_3$, and $KZnF_3$, a small peak is observed between the peaks at about 16 and 6 eV in RBE.

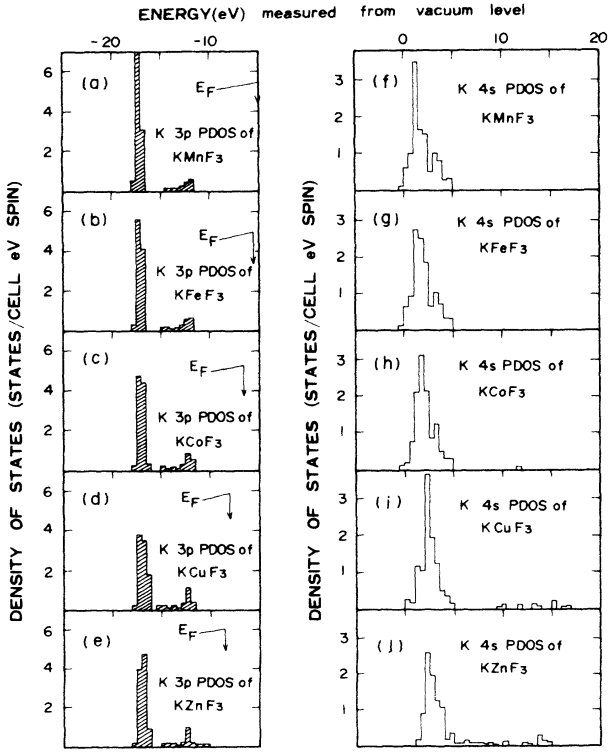

FIG. 8. Partial density of states (PDOS) for $3p$ orbital [(a) $KMnF_3$, (b) $KFeF_3$, (c) $KCoF_3$, (d) $KCuF_3$, and (e) $KZnF_3$] and $4s$ orbital [(f) $KMnF_3$, (g) $KFeF_3$, (h) $KCoF_3$, (i) $KCuF_3$, and (j) $KZnF_3$] of K^+ ion in KMF_3.

The calculated PDOS are shown for $P_{3p}^{(K)}$ and $P_{4s}^{(K)}$ in Fig. 8, for $P_{4s}^{(M)}$, $P_{4p}^{(M)}$, and $P_{3d}^{(M)}$ in Fig. 9, and for $P_{2s}^{(F)}$ in Fig. 10 and for $P_{2p}^{(F)}$ in Fig. 11. Figure 9 also includes the experimental metal K x-ray-absorption spectra by Shulman *et al.* The correspondence between these experimental results and the $P_{4p}^{(M)}$ (M=Mn, Fe, Co, and Zn) is fairly satisfactory. Especially, the absence of the structure A' in $KZnF_3$ is correctly predicted from our band approach. This is due to the fact that in $KZnF_3$ there is no unoccupied $3d$ band with metal $4p$ states mixed, as seen from Figs. 9(n) and 9(o). Figure 11(d) shows a comparison between the PDOS of F $2p$ and the F $K\alpha$ emission spectrum for $KCuF_3$ observed by Kawada, which are in good agreement with each other.

At the end of this section, we would like to mention the change of the DOS with the variation of metal ions. From the results of the TODS in Figs. 3(a) and 7 we see that the F $2s$, K $3p$, and F $2p$ bands almost do not change from compound to compound, but the metal $3d$ band shifts to the low-energy side with the increasing atomic number of the metal. This energy shift of the $3d$ band well corresponds to that of the Madelung corrected $3d$ level of the metal ion. The energy gap between the F $2p$ and metal $3d$ bands decreases in going from $KMnF_3$ to $KCuF_3$ and eventually vanishes in $KZnF_3$. This behavior is also found in the $P_{2p}^{(F)}$ shown in Figs. 6(b) and 11. The experimental study of the F $K\alpha$ emission for a series of perovskite-type compounds is highly desired in order to verify such a systematic change experimentally. Such an experiment would clarify a question about a many-body effect near the Fermi level described in Sec. III A, because our result for $KMnF_3$ [Fig. 11(a)] suggests no peak at the high-energy side of the main peak of the F $K\alpha$ emission spectrum

IV. SUMMARY

We have calculated the band structures for perovskite-type compounds KMF_3 (M=Mn, Fe, Co, Ni, Cu, and Zn) on the basis of the extended Hückel tight-binding method and presented the total and partial densities of states. From comparisons of these densities of states with experimental data from ultraviolet photoelectron and x-ray spectroscopies, it has been shown that our calculated results are in good agreement with those experiments involving information even on conduction bands. This is surprising, because it is believed that an energy-band calculation by a linear combination of atomic orbitals method leads to good valence bands, but does not necessarily lead to good conduction bands. We think that the reason for our success lies in the following points: (1)

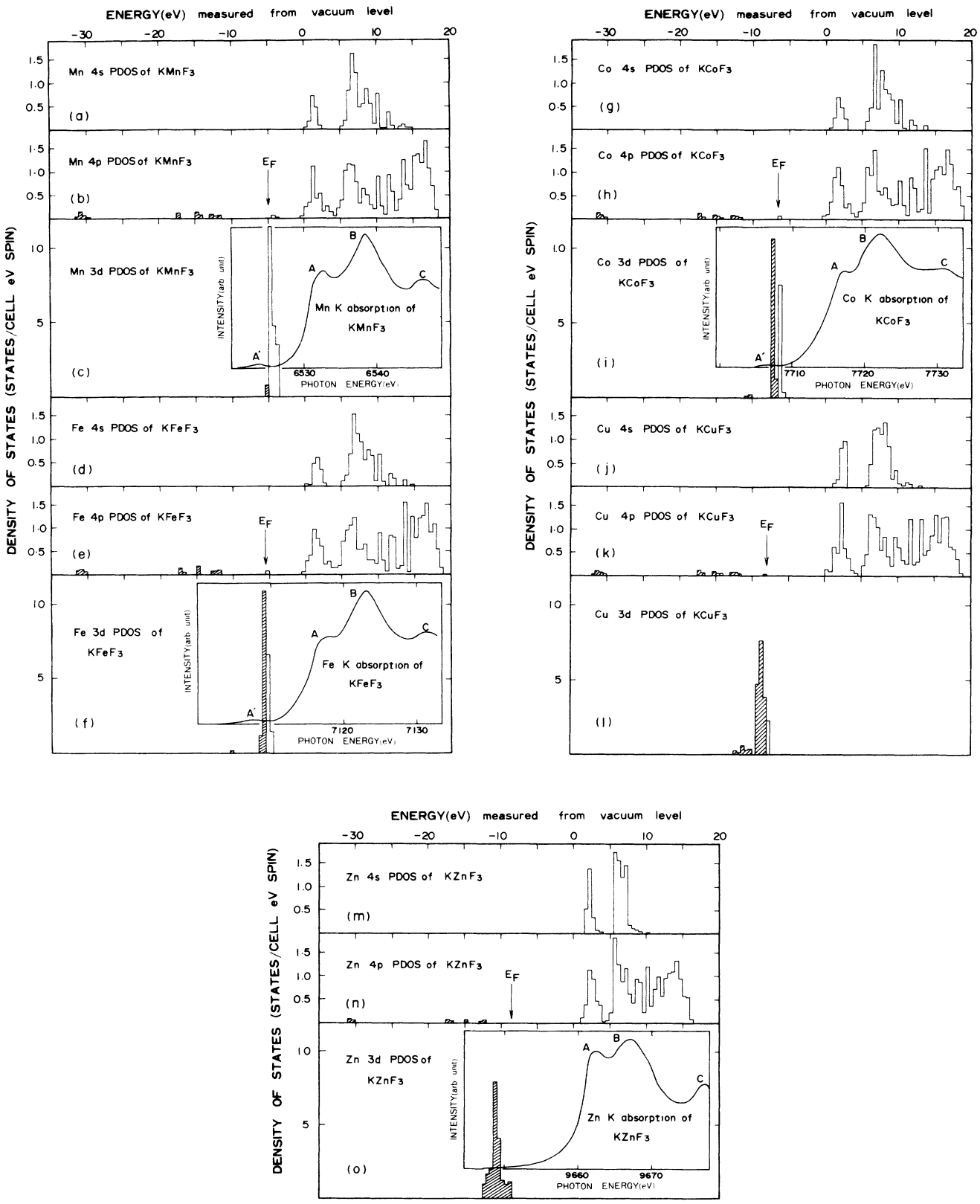

FIG. 9. Partial density of states (PDOS) for 4*s*, 4*p*, and 3*d* orbitals of M^{2+} ion in KMF_3. (a)–(c) show the results for $KMnF_3$; (d)–(f), those for $KFeF_3$; (g)–(i), those for $KCoF_3$; (j)–(l), those for $KCuF_3$; and (m)–(o), those for $KZnF_3$. Metal K x-ray-absorption spectra observed by Shulman *et al.* are also illustrated for KMF_3 (M=Mn, Fe, Co, and Zn).

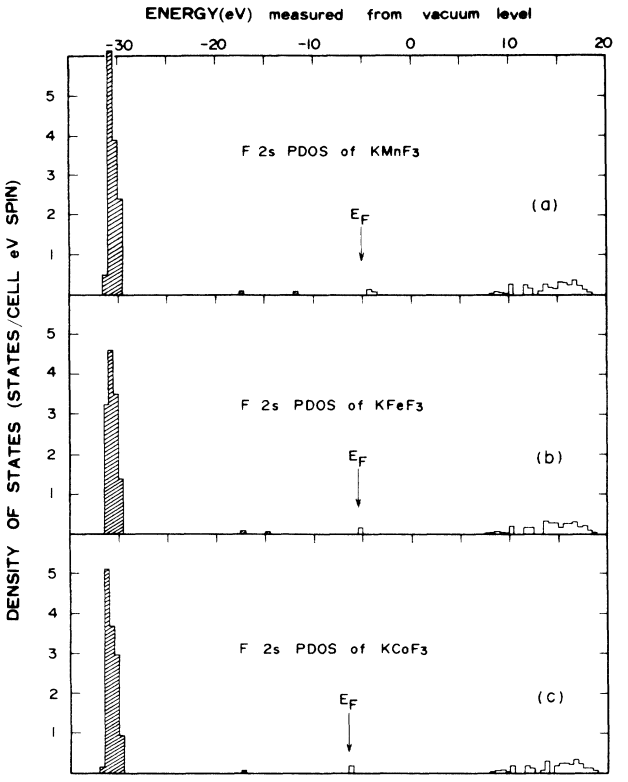

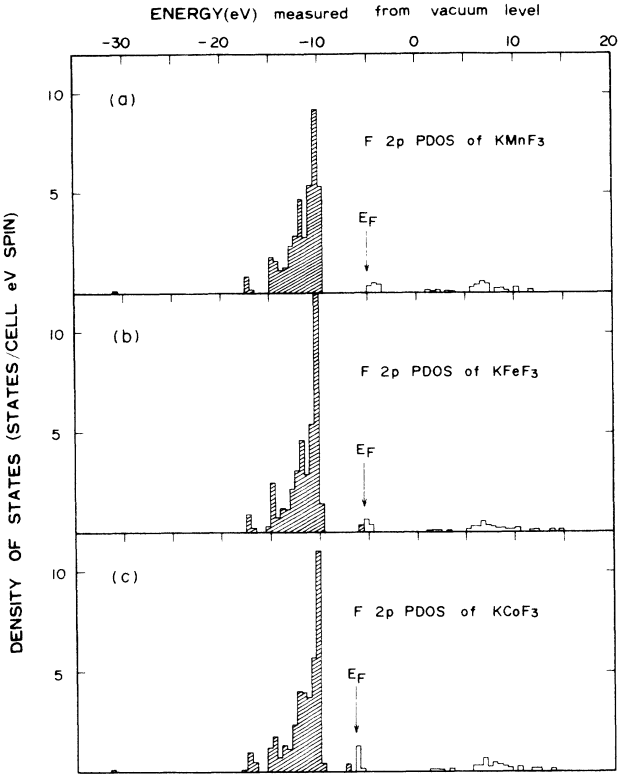

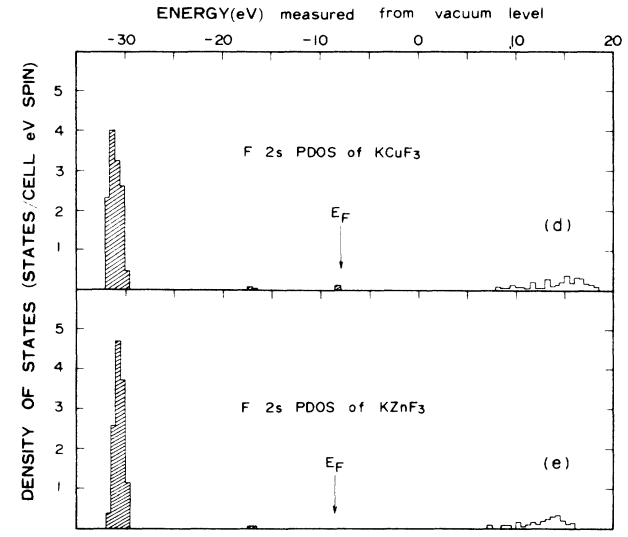

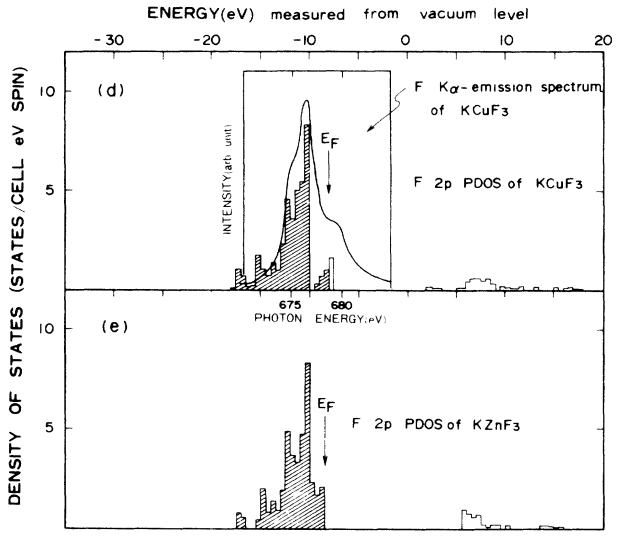

FIG. 10. Partial density of states (PDOS) for the 2*s* orbital of the F^- ion in (a) $KMnF_3$, (b) $KFeF_3$, (c) $KCoF_3$, (d) $KCuF_3$, and (e) $KZnF_3$.

FIG. 11. Partial density of states (PDOS) for the 2*p* orbital of the F^- ion in (a) $KMnF_3$, (b) $KFeF_3$, (c) $KCoF_3$, (d) $KCuF_3$, and (e) $KZnF_3$. F $K\alpha$ emission spectrum for $KCuF_3$ observed by Kawada is shown in (d).

atomic data obtained from self-consistent-field calculations are used instead of empirical atomic ones and (2) matrix elements, obtained by carrying out the summation up to a large enough distance for overlap integrals to be negligibly small, are adopted for the secular equation which determines band structures.

From the results for a hypothetical band-structure calculation in which the contribution of potassium ions is neglected, we have pointed out that in the metal K x-ray-absorption spectra for KMF_3, a structure appearing at the low-energy side of the main peak is closely related to the potassium ions. This result is consistent with interpretations in our recent calculations based on the multiple-scattering theory for perovskite-type compounds and Co^{3+} complex ones.

APPENDIX A

In Tables II–IV, we present the shell structures necessary for the calculations of overlap integrals, for the perovskite-type compound $A^+B^{2+}C_3^-$, along with the absolute values of the basis overlap integrals ($\Delta_{sp\sigma}^{\mu,\nu}, \Delta_{pp\sigma}^{\mu,\nu}, \Delta_{pp\pi}^{\mu,\nu}, \ldots$) for $KNiF_3$ and the values of σ_μ. The shell structures are characterized by the distance (in units of lattice constant) from a central atom (denoted by the zeroth shell), the number of atoms, and the kind of atoms. The basic overlap integrals are calculated by using the atomic orbitals of $3p$ and $4s$ for K^+, $3d$, $4s$, and $4p$ for Ni^{2+} and $2s$ and $2p$ for F^-, which are obtained from self-consistent-field calculations. The Madelung correction is given by $(2/a_0)\sigma_\mu$ ($\mu = A^+, B^{2+}$, and C^-).

TABLE II. For A atom: $\sigma_A = 2.695$ ($\mu = A$).

Shell	Number [Kind (ν)]	Distance	$\lvert\Delta_{ss\sigma}^{\mu,\nu}\rvert$	$\lvert\Delta_{sp\sigma}^{\mu,\nu}\rvert$	$\lvert\Delta_{sd\sigma}^{\mu,\nu}\rvert$	$\lvert\Delta_{pp\sigma}^{\mu,\nu}\rvert$	$\lvert\Delta_{pp\pi}^{\mu,\nu}\rvert$	$\lvert\Delta_{pd\sigma}^{\mu,\nu}\rvert$	$\lvert\Delta_{pd\pi}^{\mu,\nu}\rvert$
0	1(A)	0	1	0		1	1		
1	12(C)	$\sqrt{2}/2$	1.396×10^{-1}	1.701×10^{-1}		7.692×10^{-2}	2.526×10^{-2}		
2	8(B)	$\sqrt{3}/2$	2.126×10^{-1}	2.568×10^{-1}	2.074×10^{-2}	8.831×10^{-2}	1.758×10^{-2}	1.058×10^{-2}	2.314×10^{-3}
3	6(A)	1	2.726×10^{-1}	5.459×10^{-2}		5.384×10^{-3}	4.936×10^{-4}		
4	24(C)	$\sqrt{6}/2$	1.349×10^{-2}	5.291×10^{-2}		7.120×10^{-3}	6.683×10^{-4}		
5	12(A)	$\sqrt{2}$	7.715×10^{-2}	8.921×10^{-3}		3.214×10^{-5}	1.231×10^{-6}		
6	24(C)	$\sqrt{10}/2$	8.814×10^{-4}	1.153×10^{-2}		2.435×10^{-4}	1.165×10^{-5}		
7	24(B)	$\sqrt{11}/2$	4.562×10^{-3}	1.418×10^{-2}	8.457×10^{-4}	4.029×10^{-4}	2.454×10^{-5}	0	0
8	8(A)	$\sqrt{3}$	2.012×10^{-2}	8.333×10^{-4}		0	0		
9	48(C)	$\sqrt{14}/2$	2.574×10^{-5}	2.105×10^{-3}		2.178×10^{-6}	0		
10	6(A)	2	4.755×10^{-3}	4.480×10^{-5}		0	0		
11	36(C)	$3\sqrt{2}/2$	0	3.329×10^{-4}		0	0		
12	24(B)	$\sqrt{19}/2$	4.250×10^{-5}	4.422×10^{-4}	1.663×10^{-6}	0	0	0	0
13	24(A)	$\sqrt{5}$	1.038×10^{-3}	0		0	0		
14	24(C)	$\sqrt{22}/2$	0	3.345×10^{-5}		0	0		
15	24(A)	$\sqrt{6}$	1.981×10^{-4}	0		0	0		
16	72(C)	$\sqrt{26}/2$	0	0		0	0		
17	32(B)	$3\sqrt{3}/2$	0	1.076×10^{-5}	0	0	0	0	0
18	48(C)	$\sqrt{30}/2$	0	0		0	0		
19	12(A)	$2\sqrt{2}$	1.746×10^{-6}	0		0	0		
20	48(C)	$\sqrt{34}/2$	0	0		0	0		
21	48(B)	$\sqrt{35}/2$	0	0	0	0	0	0	0
22	30(A)	3	0	0		0	0		

TABLE III. For B atom: $\sigma_B = 6.194$ ($\mu = B$).

Shell	Number [Kind (ν)]	Distance	$\lvert\Delta^{\mu,\nu}_{ss\sigma}\rvert$	$\lvert\Delta^{\mu,\nu}_{sp\sigma}\rvert$	$\lvert\Delta^{\mu,\nu}_{sd\sigma}\rvert$	$\lvert\Delta^{\mu,\nu}_{pp\sigma}\rvert$	$\lvert\Delta^{\mu,\nu}_{pp\pi}\rvert$	$\lvert\Delta^{\mu,\nu}_{pd\sigma}\rvert$	$\lvert\Delta^{\mu,\nu}_{pd\pi}\rvert$	$\lvert\Delta^{\mu,\nu}_{dd\sigma}\rvert$	$\lvert\Delta^{\mu,\nu}_{dd\pi}\rvert$	$\lvert\Delta^{\mu,\nu}_{dd\delta}\rvert$
0	1(B)	0	1	0	0	1	1	0	0	1	1	1
1	6(C)	1/2	1.842×10^{-1}	2.848×10^{-1}		2.107×10^{-1}	2.128×10^{-1}					
2	8(A)	$\sqrt{3}/2$	2.126×10^{-1}	3.878×10^{-2}		8.831×10^{-2}	1.758×10^{-2}					
3	6(B)	1	3.665×10^{-2}	9.237×10^{-2}	7.414×10^{-3}	1.710×10^{-1}	3.669×10^{-2}	1.773×10^{-2}	4.981×10^{-3}	1.999×10^{-3}	5.672×10^{-4}	4.651×10^{-5}
4	24(C)	$\sqrt{5}/2$	1.591×10^{-3}	2.839×10^{-2}		5.819×10^{-2}	1.046×10^{-2}					
5	12(B)	$\sqrt{2}$	1.510×10^{-3}	7.864×10^{-3}	1.961×10^{-4}	2.393×10^{-2}	2.809×10^{-3}	1.247×10^{-3}	2.071×10^{-4}	1.437×10^{-5}	1.715×10^{-6}	0
6	30(C)	3/2	1.064×10^{-5}	2.176×10^{-3}		8.256×10^{-3}	8.092×10^{-4}					
7	24(A)	$\sqrt{11}/2$	4.562×10^{-3}	1.316×10^{-5}		4.029×10^{-4}	2.454×10^{-5}					
8	8(B)	$\sqrt{3}$	5.544×10^{-5}	7.361×10^{-4}	2.509×10^{-6}	3.520×10^{-3}	2.843×10^{-4}	1.116×10^{-4}	1.102×10^{-5}	0	0	0
9	24(C)	$\sqrt{13}/2$	0	1.277×10^{-4}		1.033×10^{-3}	7.177×10^{-5}					
10	6(B)	2	1.003×10^{-6}	6.613×10^{-5}	0	5.169×10^{-4}	3.183×10^{-5}	6.620×10^{-6}	0	0	0	0
11	48(C)	$\sqrt{17}/2$	0	3.187×10^{-6}		1.311×10^{-4}	6.666×10^{-6}					
12	24(A)	$\sqrt{19}/2$	4.250×10^{-5}	0		0	0					
13	24(B)	$\sqrt{5}$	0	5.075×10^{-6}	0	7.628×10^{-5}	3.762×10^{-6}	0	0	0	0	0
14	48(C)	$\sqrt{21}/2$	0	0		1.434×10^{-5}	0					
15	24(B)	$\sqrt{6}$	0	0	0	1.111×10^{-5}	0	0	0	0	0	0
16	30(C)	5/2	0	0		0	0					
17	32(A)	$3\sqrt{3}/2$	0	0		0	0					
18	72(C)	$\sqrt{29}/2$	0	0		0	0					
19	12(B)	$2\sqrt{2}$	0	0	0	0	0	0	0	0	0	0
20	48(C)	$\sqrt{33}/2$	0	0		0	0					
21	48(A)	$\sqrt{35}/2$	0	0		0	0					
22	30(B)	3	0	0	0	0	0	0	0	0	0	0

TABLE IV. For C atom: $\sigma_C = -3.233$ ($\mu = C$).

Shell	Number [Kind (ν)]	Distance	$\lvert\Delta^{\mu,\nu}_{ss\sigma}\rvert$	$\lvert\Delta^{\mu,\nu}_{sp\sigma}\rvert$	$\lvert\Delta^{\mu,\nu}_{sd\sigma}\rvert$	$\lvert\Delta^{\mu,\nu}_{pp\sigma}\rvert$	$\lvert\Delta^{\mu,\nu}_{pp\pi}\rvert$	$\lvert\Delta^{\mu,\nu}_{pd\sigma}\rvert$	$\lvert\Delta^{\mu,\nu}_{pd\pi}\rvert$
0	1(C)	0	1	0		1	1		
1	2(B)	1/2	1.842×10^{-1}	3.362×10^{-1}	6.729×10^{-2}	2.107×10^{-1}	2.128×10^{-1}	6.390×10^{-2}	5.242×10^{-2}
2	4(A)	$\sqrt{2}/2$	1.396×10^{-1}	2.367×10^{-2}		7.692×10^{-2}	2.526×10^{-2}		
2	8(C)	$\sqrt{2}/2$	5.607×10^{-3}	6.397×10^{-2}		9.350×10^{-2}	4.573×10^{-2}		
3	6(C)	1	1.080×10^{-4}	1.433×10^{-2}		5.023×10^{-2}	1.146×10^{-2}		
4	8(B)	$\sqrt{5}/2$	1.591×10^{-3}	9.396×10^{-3}	1.425×10^{-4}	5.819×10^{-2}	1.046×10^{-2}	5.663×10^{-3}	1.452×10^{-3}
5	8(A)	$\sqrt{6}/2$	1.349×10^{-2}	4.413×10^{-5}		7.120×10^{-3}	6.683×10^{-4}		
5	16(C)	$\sqrt{6}/2$	1.045×10^{-6}	2.217×10^{-3}		2.062×10^{-2}	2.965×10^{-3}		
6	12(C)	$\sqrt{2}$	0	2.595×10^{-4}		7.452×10^{-3}	8.198×10^{-4}		
7	10(B)	3/2	1.064×10^{-5}	4.669×10^{-4}	0	8.265×10^{-3}	8.092×10^{-4}	3.560×10^{-4}	3.606×10^{-5}
8	8(A)	$\sqrt{10}/2$	8.814×10^{-4}	0		2.435×10^{-4}	1.165×10^{-5}		
8	16(C)	$\sqrt{10}/2$	0	2.363×10^{-5}		2.741×10^{-3}	2.310×10^{-4}		
9	8(C)	$\sqrt{3}$	0	0		9.586×10^{-4}	6.088×10^{-5}		
10	8(B)	$\sqrt{13}/2$	0	1.618×10^{-5}	0	1.033×10^{-3}	7.177×10^{-5}	6.662×10^{-6}	0
11	16(A)	$\sqrt{14}/2$	2.574×10^{-5}	0		2.178×10^{-6}	0		
11	32(C)	$\sqrt{14}/2$	0	0		2.952×10^{-4}	1.367×10^{-5}		
12	6(C)	2	0	0		7.123×10^{-5}	2.274×10^{-6}		
13	16(B)	$\sqrt{17}/2$	0	0	0	1.311×10^{-4}	6.666×10^{-6}	0	0
14	12(A)	$3\sqrt{2}/2$	0	0		0	0		
14	24(C)	$3\sqrt{2}/2$	0	0		1.049×10^{-5}	0		
15	24(C)	$\sqrt{5}$	0	0		0	0		
16	16(B)	$\sqrt{21}/2$	0	0	0	1.434×10^{-5}	0	0	0
17	8(A)	$\sqrt{22}/2$	0	0		0	0		
17	16(C)	$\sqrt{22}/2$	0	0		0	0		
18	24(C)	$\sqrt{6}$	0	0		0	0		
19	10(B)	5/2	0	0	0	0	0	0	0
20	24(A)	$\sqrt{26}/2$	0	0		0	0		
20	48(C)	$\sqrt{26}/2$	0	0		0	0		
21	24(B)	$\sqrt{29}/2$	0	0	0	0	0	0	0
22	16(A)	$\sqrt{30}/2$	0	0		0	0		
22	32(C)	$\sqrt{30}/2$	0	0		0	0		
23	12(C)	$2\sqrt{2}$	0	0		0	0		
24	16(B)	$\sqrt{33}/2$	0	0	0	0	0	0	0
25	16(A)	$\sqrt{34}/2$	0	0		0	0		
25	32(C)	$\sqrt{34}/2$	0	0		0	0		
26	30(C)	3	0	0		0	0		

APPENDIX B

In Tables V–X, we present results of the MO for a $(MF_6)^{4-}$ cluster in perovskite-type compounds KMF_3 (M=Mn, Fe, Co, Ni, Cu, and Zn). $n(\Gamma)$ is the occupation number of electrons on MO. The energy is measured from the vacuum level. For the definition of the coefficient u's of the MO, see Ref. 15.

TABLE V. $(MnF_6)^{4-}$.

Γ	Energy (eV)	$n(\Gamma)$	u_1	u_2	u_3	u_4
$4t_{1u}$	12.6	0	−1.29	−0.483	0.319	0.280
$3a_{1g}$	9.07	0	1.37	−0.472	0.601	
$3e_g$	−3.95	0	1.02	0.178	−0.280	
$2t_{2g}$	−4.88	5	1.01	−0.152		
$1t_{1g}$	−10.6	6	1.00			
$2e_g$	−11.1	4	0.125	−0.0762	0.975	
$3t_{1u}$	−11.2	6	−0.0159	0.0818	−0.897	0.507
$1t_{2u}$	−11.3	6	1.00			
$1t_{2g}$	−13.0	6	0.0301	0.996		
$2t_{1u}$	−13.2	6	0.191	−0.0754	−0.491	−0.923
$2a_{1g}$	−13.7	2	0.160	0.158	1.09	
$1e_g$	−29.7	4	0.00744	−0.997	−0.0274	
$1t_{1u}$	−30.3	6	−0.137	−1.05	0.0428	0.107
$1a_{1g}$	−30.4	2	0.0777	−1.02	0.107	

TABLE VI. $(FeF_6)^{4-}$.

Γ	Energy (eV)	$n(\Gamma)$	u_1	u_2	u_3	u_4
$4t_{1u}$	12.8	0	−1.30	−0.491	0.316	0.291
$3a_{1g}$	9.07	0	1.37	−0.475	0.617	
$3e_g$	−5.03	0	1.01	0.178	−0.299	
$2t_{2g}$	−5.92	6	1.01	−0.162		
$1t_{1g}$	−10.7	6	1.00			
$2e_g$	−11.3	4	0.158	−0.0758	0.968	
$3t_{1u}$	−11.3	6	−0.0205	0.0850	−0.901	0.498
$1t_{2u}$	−11.5	6	1.00			
$1t_{2g}$	−13.2	6	0.0456	0.994		
$2t_{1u}$	−13.4	6	0.191	−0.0828	−0.479	−0.931
$2a_{1g}$	−13.9	2	0.154	0.171	1.09	
$1e_g$	−29.9	4	0.0125	−0.996	−0.0296	
$1t_{1u}$	−30.5	6	−0.137	−1.05	0.0406	0.112
$1a_{1g}$	−30.6	2	0.0738	−1.01	0.108	

TABLE VII. $(CoF_6)^{4-}$.

Γ	Energy (eV)	$n(\Gamma)$	u_1	u_2	u_3	u_4
$4t_{1u}$	12.8	0	−1.30	−0.494	0.326	0.290
$3a_{1g}$	8.98	0	1.38	−0.472	0.640	
$3e_g$	−6.28	1	−0.995	−0.169	0.344	
$2t_{2g}$	−7.13	6	1.00	−0.163		
$1t_{1g}$	−10.7	6	1.00			
$3t_{1u}$	−11.4	6	−0.0221	0.0887	−0.903	0.493
$2e_g$	−11.5	4	0.211	−0.0730	0.952	
$1t_{2u}$	−11.6	6	1.00			
$1t_{2g}$	−13.4	6	0.0620	0.992		
$2t_{1u}$	−13.6	6	0.191	−0.0888	−0.475	−0.934
$2a_{1g}$	−14.0	2	0.145	0.184	1.08	
$1e_g$	−30.0	4	0.0171	−0.995	−0.0314	
$1t_{1u}$	−30.7	6	−0.136	−1.04	0.0400	0.114
$1a_{1g}$	−30.8	2	0.0687	−1.01	0.108	

TABLE VIII. $(NiF_6)^{4-}$.

Γ	Energy (eV)	$n(\Gamma)$	u_1	u_2	u_3	u_4
$4t_{1u}$	13.0	0	−1.31	−0.499	0.335	0.290
$3a_{1g}$	8.93	0	1.39	−0.472	0.655	
$3e_g$	−7.22	2	−0.980	−0.174	0.382	
$2t_{2g}$	−8.09	6	1.00	−0.182		
$1t_{1g}$	−10.8	6	1.00			
$3t_{1u}$	−11.6	6	−0.0239	0.0928	−0.904	0.489
$2e_g$	−11.6	4	0.262	−0.0683	0.936	
$1t_{2u}$	−11.7	6	1.00			
$1t_{2g}$	−13.6	6	0.0837	0.988		
$2t_{1u}$	−13.8	6	0.192	−0.0954	−0.471	−0.937
$2a_{1g}$	−14.1	2	0.138	0.196	1.08	
$1e_g$	−30.1	4	0.0217	−0.994	−0.0333	
$1t_{1u}$	−30.8	6	−0.136	−1.04	0.0399	0.117
$1a_{1g}$	−31.0	2	0.0646	−1.01	0.109	

TABLE IX. $(CuF_6)^{4-}$.

Γ	Energy (eV)	$n(\Gamma)$	u_1	u_2	u_3	u_4
$4t_{1u}$	12.5	0	−1.30	−0.493	0.347	0.282
$3a_{1g}$	8.23	0	1.39	−0.457	0.677	
$3e_g$	−8.20	3	−0.952	−0.167	0.455	
$2t_{2g}$	−9.09	6	0.998	−0.189		
$1t_{1g}$	−10.9	6	1.00			
$3t_{1u}$	−11.6	6	−0.0247	0.0938	−0.904	0.489
$1t_{2u}$	−11.7	6	1.00			
$2e_g$	−11.8	4	0.344	−0.0587	0.902	
$1t_{2g}$	−13.6	6	0.104	0.986		
$2t_{1u}$	−13.8	6	0.186	−0.0975	−0.471	−0.934
$2a_{1g}$	−14.1	2	0.116	0.205	1.07	
$1e_g$	−30.1	4	0.0240	−0.994	−0.0337	
$1t_{1u}$	−30.8	6	−0.129	−1.04	0.0379	0.112
$1a_{1g}$	−31.0	2	0.0530	−1.00	0.101	

TABLE X. $(ZnF_6)^{4-}$.

Γ	Energy (eV)	$n(\Gamma)$	u_1	u_2	u_3	u_4
$4t_{1u}$	10.9	0	−1.28	−0.467	0.362	0.262
$3a_{1g}$	6.29	0	1.36	−0.418	0.700	
$3e_g$	−9.67	4	0.823	0.151	−0.667	
$2t_{2g}$	−10.8	6	0.988	−0.232		
$1t_{1g}$	−10.8	6	1.00			
$3t_{1u}$	−11.5	6	−0.0246	0.0894	−0.900	0.495
$1t_{2u}$	−11.6	6	1.00			
$2e_g$	−12.1	4	−0.583	0.0243	−0.756	
$2t_{1u}$	−13.5	6	0.167	−0.0940	−0.475	−0.923
$1t_{2g}$	−13.5	6	0.168	0.975		
$2a_{1g}$	−13.8	2	0.0645	0.209	1.05	
$1e_g$	−30.0	4	0.0250	−0.995	−0.0316	
$1t_{1u}$	−30.5	6	−0.109	−1.03	0.0322	0.0959
$1a_{1g}$	−30.8	2	0.0290	−0.996	0.0819	

[1]S. Sugano and R. G. Shulman, Phys. Rev. **130**, 517 (1963).
[2]B. Kleinman and M. Karplus, Phys. Rev. B **3**, 24 (1971).
[3]T. F. Soules, J. W. Richardson, and D. M. Vaught, Phys. Rev. B **3**, 2186 (1971).
[4]T. F. Soules, E. J. Kelly, D. M. Vaught, and J. W. Richardson, Phys. Rev. B **6**, 1519 (1972).
[5]L. F. Mattheiss, Phys. Rev. B **6**, 4718 (1972).
[6]R. G. Shulman, Y. Yafet, P. Eisenberger, and W. E. Blumberg, Proc. Natl. Acad. Sci. U.S.A. **73**, 1384 (1976).
[7]H. Onuki, F. Sugawara, M. Hirano, and Y. Yamaguchi, J. Phys. Soc. Jpn. **49**, 2314 (1980).
[8]A. Kawada, Masters' thesis, Utsunomiya University, 1983.
[9]M. Kitamura, S. Muramatsu, and C. Sugiura, Phys. Rev. B **33**, 5294 (1986).
[10]M. Kitamura, C. Sugiura, and S. Muramtsu, Solid State Commun. **62**, 663 (1987).
[11]M. Kitamura, S. Muramatsu, and C. Sugiura, Phys. Status Solidi B **142**, 191 (1987).
[12]M. Kitamura, S. Muramatsu, and C. Sugiura, Phys. Rev. B **37**, 6486 (1988).
[13]M. Kitamura, C. Sugiura, and S. Muramatsu, Solid State Commun. **67**, 313 (1988).
[14]M. Kitamura, C. Sugiura, and S. Muramatsu, Phys. Status Solidi B **149**, 791 (1988).
[15]M. Kitamura, C. Sugiura, and S. Muramatsu, Phys. Rev. B **39**, 10288 (1989).
[16]L. A. Grunes, R. D. Leapman, C. N. Wilker, R. Hoffmann, and A. B. Kunz, Phys. Rev. B **25**, 7157 (1982).
[17]M. Wolfsberg and L. Helmholtz, J. Chem. Phys. **20**, 837 (1962).
[18]H. M. Evjen, Phys. Rev. **39**, 675 (1932).
[19]J. C. Slater and G. F. Koster, Phys. Rev. **94**, 1498 (1954).
[20]M. Kitamura, S. Muramatsu, and C. Sugiura, Phys. Rev. A **35**, 2838 (1987).
[21]F. Herman and S. Skillman, *Atomic Structure Calculations* (Prentice-Hall, Englewood Cliffs, NJ, 1963).
[22]K. Schwarz, Phys. Rev. B **5**, 2466 (1972).
[23]R. W. G. Wyckoff, *Crystal Structures* (Interscience, New York, 1960), Vol. 2.
[24]W. A. Harrison, *Electronic Structure and the Properties of Solid, The Physics of the Chemical Bond* (Freeman, San Francisco, 1980).
[25]L. C. Cusachs, J. Chem. Phys. **43**, S157 (1965).